Polymer Testing 143 (2025) 108714

Contents lists available at ScienceDirect

Polymer Testing

journal homepage: www.elsevier.com/locate/polytest

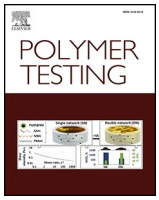

Nanoindentation analysis of transcrystalline layers in model carbon fiber-reinforced PEEK composite

Sophie Vanpée [a,b,*], Bernard Nysten [b], Jérémy Chevalier [c], Thomas Pardoen [a,d,**]

[a] Institute of Mechanics, Materials and Civil Engineering (iMMC), UCLouvain, Place Sainte-Barbe 2, 1348, Louvain-la-Neuve, Belgium
[b] Institute of Condensed Matter and Nanosciences (IMCN), UCLouvain, Croix du Sud 1, 1348, Louvain-la-Neuve, Belgium
[c] Material Science Application Center (MSAC), Syensqo, Rue de la Fusée 98, 1130, Brussels, Belgium
[d] WEL Research Institute, Avenue Pasteur 6, 1300, Wavre, Belgium

ARTICLE INFO

Keywords:
Semi-crystalline composite
Microstructure
Nanoindentation
Atomic force microscopy

ABSTRACT

Nanoindentation (NI) and atomic force microscopy (AFM) nanoindentation, coupled with polarized light microscopy (PLM), were used to determine the nano-/micromechanical behavior of the amorphous regions and individual crystalline structures, both spherulites and transcrystalline (TC) layers, in PEEK samples containing few carbon fibers. To this aim, thin model samples with a controlled thickness were manufactured to allow both microstructure characterization in transmission mode and indentation tests without substrate effects. Surface roughness of the model samples was carefully minimized to get reliable and low dispersion from indentation experiments. The artefacts and sources of uncertainty of performing indentation experiments on thin polymer films containing some fibers are also discussed. The AFM nanoindentation added value is the possibility of evaluating the mechanical behavior of crystalline structures at the nanoscale, for the determination of mechanical behavior heterogeneities at the intra-spherulitic and intra-transcrystalline scale.

1. Introduction

Although the relationship between microstructure and properties of semi-crystalline thermoplastics in the context of fiber-reinforced composites has been the subject of extensive researches for many years, several questions remain unresolved in particular regarding the local heterogeneous mechanical behavior of the interfiber zone as a function of the matrix microstructure. However, this is a key information to guide the optimization of the composite properties but also for the establishment of more predictive multiscale models which requires at the lowest length scale a good understanding of the polymer matrix mechanical response. The matrix microstructure is directly linked to the thermal cycles experienced by the composite part during manufacturing.

Today, nano- and microscale characterization techniques can be mobilized to unravel the mechanisms of deformation and fracture at the scale of the interfiber zones. For example, different experimental methods have been developed to determine the strength of the matrix/fiber interface such as single fiber fragmentation test [1], the micro-droplet test [2], the single fiber pull-out test [3] and the fiber push-in or push-out tests [4,5]. In addition, a nano-digital image correlation (DIC) method has recently been proposed in order to directly characterize the strain field at the constituent scale during mechanical testing [6]. Finally, indentation methods such as performed with a nanoindenter (NI) and an atomic force microscope (AFM) using mechanical modes are used to determine the (visco-)elastic and (visco-)plastic properties at the micro- and nanoscale of polymers in bulk form [7–10], or in-situ when used as matrix in composites [11,12], and/or to identify the presence of potential interphases at the composite fiber/-matrix interfaces [12–16]. The mechanical properties are interrogated by indenting the surface of the material at a predefined load with tips of various dimensions. The nanoindenter tips can have a radius of few hundreds of nanometers up to several tens of micrometers [17]. The AFM tips have a smaller tip radius ranging from few nanometers up to some tens of nanometers [17], allowing the identification of the mechanical properties at a smaller length scale but with more potential experimental bias.

For instance, nanoindentation experiments performed on semi-crystalline polymers and matrices aimed at linking mechanical

* Corresponding author. Institute of Mechanics, Materials and Civil Engineering (iMMC), UCLouvain, Place Sainte-Barbe 2, 1348 Louvain-la-Neuve, Belgium.
** Corresponding author. Institute of Mechanics, Materials and Civil Engineering (iMMC), UCLouvain, Place Sainte-Barbe 2, 1348 Louvain-la-Neuve, Belgium.
E-mail addresses: sophie.vanpee@uclouvain.be (S. Vanpée), bernard.nysten@uclouvain.be (B. Nysten), jeremy.chevalier@syensqo.com (J. Chevalier), thomas.pardoen@uclouvain.be (T. Pardoen).

https://doi.org/10.1016/j.polymertesting.2025.108714
Received 6 November 2024; Received in revised form 3 January 2025; Accepted 16 January 2025
Available online 17 January 2025

properties with the degree of crystallinity [9,10,18], at capturing the gradient of mechanical behavior across sample thickness [18–20], at identifying the potential improvement of the mechanical behavior when adding reinforcing elements in the matrix [21] and/or at the identification of a potential interphase at the fiber/matrix interface of composites [21,22]. Some studies already used nanoindentation in bulk polymers to directly relate the morphology of individual crystalline entities (spherulitic or non-spherulitic structure) with their mechanical behavior using nanoindentation [23]. The identification of individual crystalline entities was possible using an optical microscope by revealing the crystalline morphology via chemical etching [23] or by re-melting and re-crystallizing the previously polished sample [24] or using polarized light microscopy for thin films (thickness between 8 and 150 μm) [25]. The topography of the samples surface was analyzed using AFM to verify that the surface roughness was sufficiently smooth to extract reliable results from nanoindentation experiment [25]. The test samples were not systematically polished prior to indentation since polishing erases a layer of material, destroys the polymer microstructure and induces hardening of the near surface region [10]. For example, it was shown that, in the particular case of PEEK, polishing can lead to an overestimation of the hardness by up to 10 % at low indentation depths (<200 nm) [10]. Although nanoindentation has been used since the 2000's to characterize composite materials [18], past studies mainly focused on amorphous polymers and matrix [12,26,27]. To the authors' knowledge, in the case of semi-crystalline composites, no studies were conducted to correlate the morphology of individual crystalline entities within the interfiber zone with their mechanical behavior.

Several advanced AFM techniques using mechanical mode are increasingly used as a nanoindentation tool to measure the nanomechanical properties of surfaces. However, only few studies applied these methods to semi-crystalline polymers in order to investigate the correlation between morphology and nanomechanical properties of crystalline entities (spherulitic and non-spherulitic structure) [28–30]. Among these studies, AFM nanoindentation has gained attention since both morphology and mechanical properties at the nanometer scale can be characterized simultaneously. The elastic modulus can be quantitatively estimated [31,32] by applying a selected load using the AFM cantilever-tip assembly and analyzing the recorded force-displacement curve with suitable models. AFM nanoindentation can potentially provide the mechanical properties of a single nanophase surrounded by a homogeneous material when performing indentation at low loads and penetration depths [33]. In the past, AFM nanoindentation has been used to determine the mechanical behavior of polymers, biomaterials, composite and composite interfaces [34–42].

According to literature, both nanoindentation and AFM using mechanical modes were mainly applied on bulk polymers. However, previous nanoindentation experiments [43,44] highlighted that the properties of the matrix differ from the bulk polymer, possibly due to differences arising in the thermal history, molecular structure and/or residual stress distribution [11,12,43–46]. In particular, in some semi-crystalline systems (PEEK/CF, …), the molecular structure of the matrix differs from the one of the bulk polymers as a result of the nucleation and growth of transcrystalline (TC) layers. "Transcrystallization" is the development of a highly oriented crystalline morphology at the fiber/matrix interface, and to the authors' knowledge, no direct local information is available regarding the influence of these TC layers on the mechanical behavior of the interfiber zone. The determination of the link between the matrix microstructure and the mechanical behavior of the interfiber zone should therefore be determined in-situ. Yet, commercial composites contain a large fiber volume fraction (≥50 %) hindering the characterization of the microstructure in the interfiber zones with conventional microscopy. The characterization of the microstructure of the matrix is crucial to understand the link between processing conditions and mechanical properties of the matrix.

Given the lack of in-situ characterization of the mechanical behavior of the interfiber zone of semi-crystalline composites and the difficulties of characterizing the matrix microstructure with optical microscopy in these zones, the goal of this study has been to set up a methodology based on classical nanoindentation and AFM nanoindentation and on a novel type of model samples that contains only a few fibers. The main advantage of testing model samples is the combined identification of individual polymer crystalline structures developed in the presence of fibers and determination of the nano- and micro-mechanical behavior of these crystalline structures using nanoindentation experiments.

The PEEK/CF system, commonly used in aerospace applications, was selected for this study as a well-known and technologically relevant semi-crystalline composite in which crystalline structures can develop at the fiber/matrix interface (i.e. TC layers) under specific conditions [47–50]. First, the microstructure of the model samples was determined by polarized light microscopy (PLM) in transmission light mode. PLM enabled the observation of the morphologies of different semi-crystalline polymers with and without fibers [48,51,52]. In a second step, PLM images were used to guide the indentation experiments (nanoindentation (NI) and atomic force microscopy in nanoindentation mode (AFM-NI)). Attention has been paid to control the thickness of the samples. Microstructure characterization with the transmission light mode requires a sample thickness relatively small but not too small in order to avoid substrate effects during indentation experiments (i.e. NI and AFM-NI). The low level of surface roughness of model samples was also verified to evaluate the reliability of nanoindentation experiments. The originality of this work resides in combining these "academic" model test specimens with advanced nanomechanical methods to investigate the local response of interfiber zones in PEEK/CF composites.

2. Materials and methods

2.1. Manufacturing of model test specimens

PEEK/CF model systems have been manufactured from PEEK pellets (KetaSpire® KT-880 NT) and carbon fibers (HexTow® AS4D 12K from Hexcel) supplied by Syensqo.

The model samples were produced as highlighted in Fig. 1. Each manufacturing step was completed as quickly as possible to avoid degradation of the polymer at high temperature (i.e. up to 400 °C).

First, ~100 mg of PEEK powder obtained after pellets grinding (Pulverisette 14, Fritsch) was spread on a glass slide. The glass slide covered by PEEK powder was then heated at 400 °C on a hot plate (Ceran™, Gestigkeit Harry™ 4A) to melt the PEEK powder. The thickness of the sample was further reduced by sliding neat glass slides on the one covered by melted PEEK. Dozens of carbon fibers with a length of ~1 cm were then placed above the melted PEEK. The impregnation of fibers by PEEK was ensured by applying pressure by adding an upper glass slide.

The model samples were then cooled down to room temperature, remelted at 400 °C to erase the thermal history and eventually isothermally crystallized on a heating plate (FP90 Central Processor and FP82 hot stage, Mettler Toledo) at high temperature (300 °C, 15 min) for generating large TC layers [49].

Finally, the upper glass slide (resp. lower glass slide) was carefully withdrawn from the sample before mechanical testing to access the upper surface (resp. back surface) of the model sample. A release agent (Loctite frekot 700 NC) was added on the withdrawn glass slides to easily remove it and access the samples without damage.

Next to model samples, a polished sample of PEEK was manufactured from the same PEEK pellets as the ones used for model sample production. The sample was first cut from a PEEK plate produced by injection molding (*FANUC, Roboshot, S-2000i150A*) and then thermally treated (i.e. quenched in a mold) before polishing. The polishing step was performed on a semi-automatic MultiPrep Precision Polishing System (Allied High Tech Products, Inc., CA, USA) with diamond lapping films coated with fixed particles of decreasing sizes (Allied High Tech

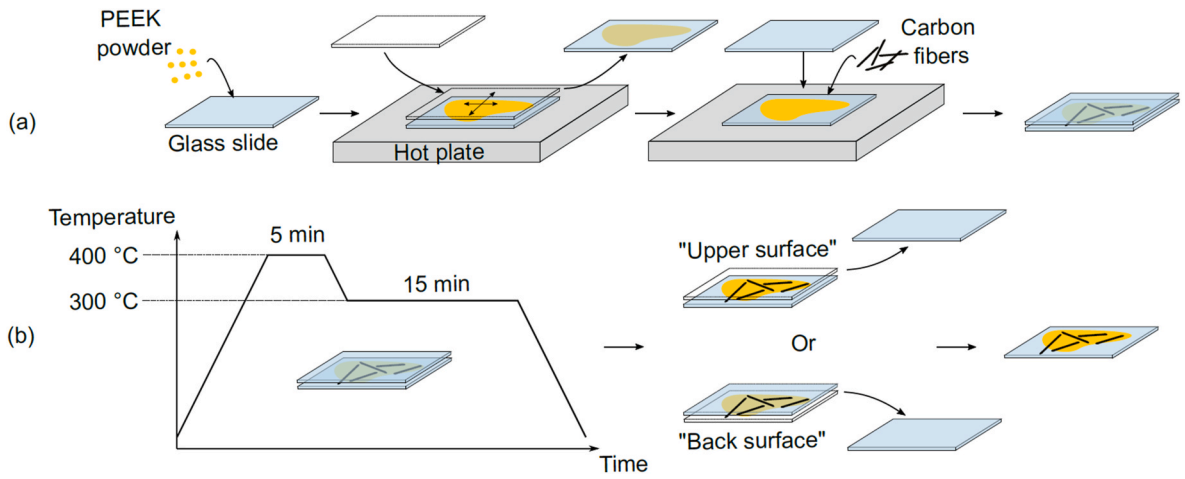

Fig. 1. Processing of model samples: manufacturing (a) and thermal treatment (b).

Products, Inc., CA, USA) going down to 0.25 μm.

2.2. Optical microscopy

The microstructure of the model samples was characterized by polarized light microscopy (PLM) in transmission light mode (Olympus AX70 light microscope) and micrographs were taken using the camera of a basic cellular phone through the lens. The regions of interest (i.e. where large TC layers were observed) were highlighted in the sample. Since observations in transmission light mode provides a sort of integrated view across the thickness of the samples, the presence of crystalline structures at the sample surface was verified prior to mechanical testing with the optical microscopes adapted in the NI and AFM instruments working in reflected light mode.

2.3. Nanoindentation

Nanoindentation (Agilent G200 nanoindenter) was performed using a Berkovich diamond tip with a half-opening angle of 65.3° and a Dynamic Contact Module (DCM II) head. The indentation tests were performed to determine mechanical properties (i.e. hardness and modulus) at different indentation depths, using the same settings as a recently published NI study on a thermoplastic polymer [12]. The tests were performed at a strain rate of 0.05 s^{-1} using the continuous stiffness measurement (CSM) mode at a frequency of 75 Hz and with a harmonic displacement of 1 nm. The load at the maximum indentation depth (i.e. 300 nm) was maintained for 10 s to minimize the viscoelastic effects during unloading. The indentation elastic modulus (E) and hardness (H) values were computed by the KLA NanoSuite software (version 6.54.0) based on the Oliver and Pharr method [53]. Nanoindentation was performed only on the upper surface of the model samples.

2.4. Atomic force microscopy in nanoindentation mode (AFM-NI)

AFM (Dimension Icon multimode AFM, Bruker Corp., USA) was performed in PeakForce Tapping mode with quantitative nanomechanical mapping (PFT-QNM) using a precalibrated ADAMA NM probe with a conical diamond tip. The cantilever spring constant, nominal tip radius and half-opening angle were 178 N m^{-1}, 13.14 nm and 45.1° respectively. The calibration of the system (detector sensitivities) was performed on sapphire prior each session of analyses.

AFM images were acquired in PFT mode with the following settings: Peak Force setpoint = 100 nN, PF frequency = 1 kHz, PF amplitude = 30 nm. Scan rates between 0.15 and 0.5 line/s were used depending on the image size.

Since only few studies report the use of AFM-NI on polymers, a parametric study was performed on a polished PEEK sample to determine the ideal experimental parameters. To this aim, indentations were performed with different maximum indentation loads (1, 2, 5 and 10 μN) and holding times (0, 1, 2, 5, 10 and 20 s). The maximum load was maintained for a given time before unloading to minimize the viscoelastic effects on the measurement of the mechanical properties (i.e. elastic modulus and hardness). The loading and unloading frequency were 1 Hz.

AFM-NI experiments were then performed on the upper and back surfaces of model samples. First, images were acquired in PFT mode. Based on these images, indentations curves were then recorded across spherulites and along lines perpendicular to fibers.

Finally, the data were processed and analyzed using home-made routines developed on Igor Pro (Wavemetrics). The force-distance curves were analyzed using the Oliver and Pharr model. The fit of the unloading curve was performed between 20 % and 98 % of the maximum load, as recommended in Refs. [54,55].

3. Results

3.1. Morphology of interfiber PEEK

A typical micrograph of the microstructure of PEEK within model

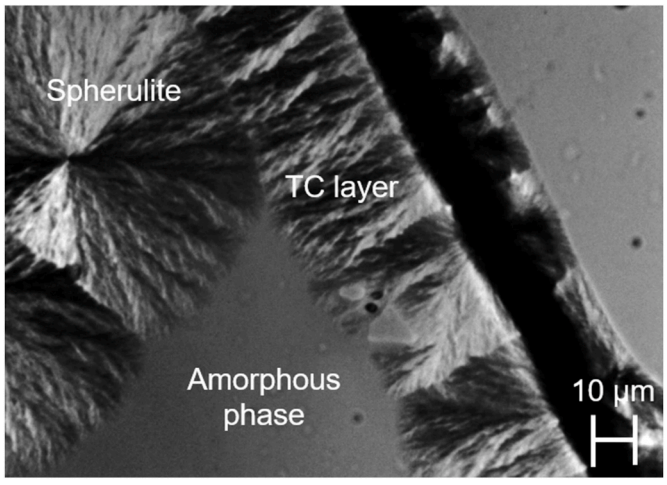

Fig. 2. Polarized light microscopy (PLM) image in transmission light mode of the model carbon fiber-reinforced PEEK sample revealing close to a fiber (in black) the three typical morphologies: “amorphous” phase, bulk spherulite and transcrystalline (TC) layer.

samples obtained by PLM in transmission light mode is shown in Fig. 2. Three different zones are identified by PLM: highly birefringent zones corresponding respectively to spherulites grown in the bulk and to transcrystalline layers grown from the fibers, and a non-birefringent zone where PEEK is expected to be amorphous or, at least, weakly crystallized. In the remaining, these zones will be referred as "spherulite", "TC layer" and "amorphous phase", respectively.

3.2. Nanoindentation of interfiber region

Fig. 3 shows (a) a topographic image obtained by AFM of an NI indent performed close to a fiber (i.e. in a TC layer) and (b) two line profiles measured across the indent. In Fig. 3(c) (resp. (d)) the NI curves of the evolution of the elastic modulus (E) (resp. the hardness (H)) as a function of the indentation depth (h) is presented for the amorphous phase, bulk spherulites and TC layers of the upper surface model samples. Indents were performed in several spherulites and TC layers in order to generate a sufficiently large number of data. The topographic image in Fig. 3(a) and the corresponding profiles (Fig. 3(b)) show no noticeable pile-up around the indent suggesting that the Oliver and Pharr model is appropriate for the analysis.

In Fig. 3(c) and (d), the dots and the error bars correspond, respectively, to the average values and the standard deviations of the values measured at 10 nm penetration depth. For all indentation depths, the TC layers exhibit mean values of E and H larger than for bulk spherulites. The amorphous phase involves the lowest levels of stiffness and hardness. At an indentation depth of 150 nm, the E (respectively H) values of the transcrystalline layers are ~ 30 % higher (resp. ~15 %) compared to spherulites which are themselves ~35 % (resp. ~ 90 %) higher compared to the amorphous phase.

Large standard deviations on E and H values are found at all indentation depths for the crystalline structures (i.e. spherulites and TC layers). The high values of E and H obtained at low indentation depths (<100 nm) can be explained by the inaccurate calibration of the tip area at small indentation depths and/or by the switch from the deformation mode of a sphere (due to tip rounding) to a pyramid [56] and/or by the presence of a thin surface layer of PEEK with higher mechanical behavior. Substrate effects (continuous increase of E/H values with h) start affecting some results from an indentation depth of 150 nm in the amorphous phase and TC layers curves of Fig. 3(c).

3.3. Atomic force microscopy

The results from the AFM indentation tests on the polished sample of PEEK are summarized in Fig. 4. Fig. 4(a) presents a topographic image of the indents produced under different maximum loads (1–10 μN from left to right) and increasing surface hold times (0–20 s from top to bottom). Fig. 4(b) shows the topographic profiles of the indent performed with $P_{max} = 5$ μN and $t_{hold} = 10$ s (parameters selected for testing the model samples). Both the topographic image and the profiles, do not reveal a clear pile-up around the indents, indicating that the Oliver and Pharr (O&P) model is suitable for the analysis. Fig. 4(c) shows the evolution of E and H obtained by fitting the unloading curves with the O&P model with the surface hold time and at the different maximum loads.

The values of E and H corresponding to the maximum indentation load tend to stabilize for a holding time of 10 s. In addition, the highest the value of the maximum load, the lowest the variation with the holding time of E and H.

Fig. 5 gathers topographic images - (a), (c) and (e) - and the values of the elastic modulus and hardness from the AFM-NI tests along the lines drawn on the corresponding images. Both images and results generated on the upper surface of the model sample (Fig. 5(a and b)) and on its back surface (Fig. 5(c–f)) are presented.

The evolution of the mechanical properties across spherulites and the

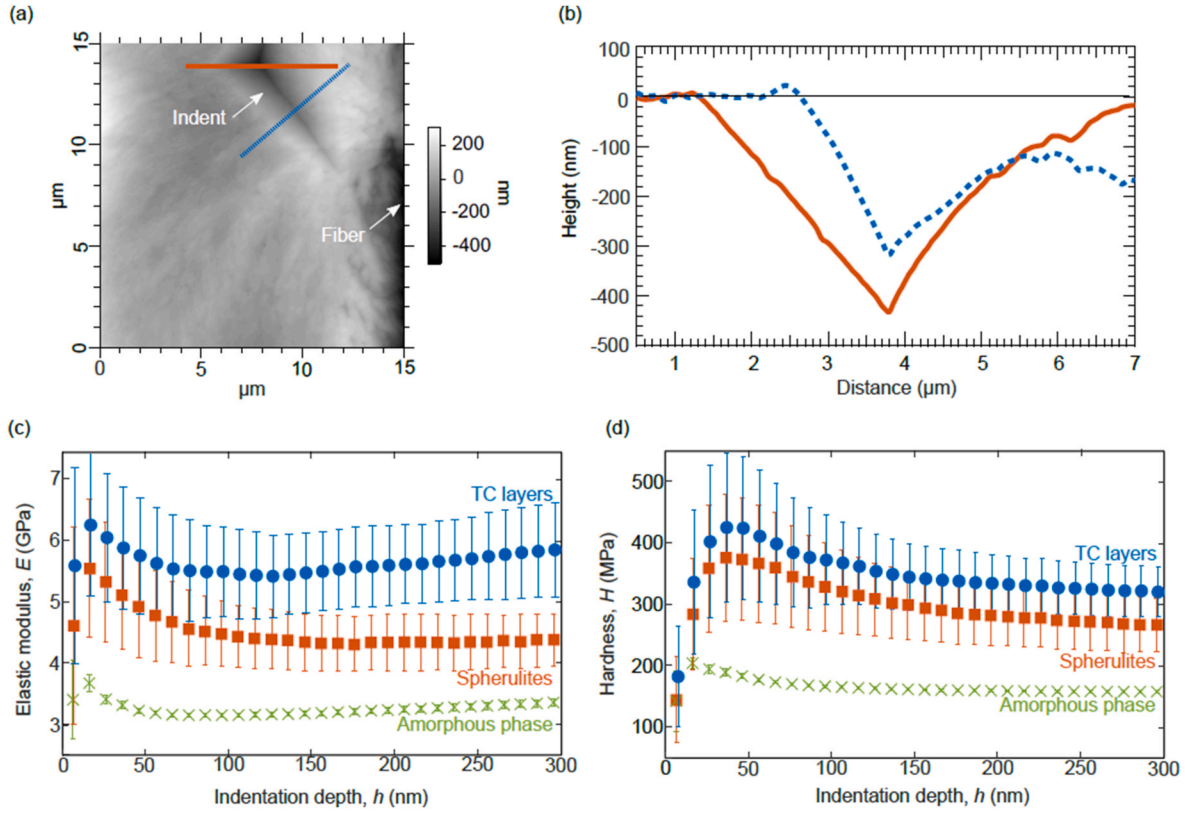

Fig. 3. (a) Atomic force microscopy (AFM) micrograph of an indent produced by the nanoindenter (NI) inside a transcrystalline (TC) layer and (b) height profiles along the orange and blue lines drawn in (a). Variation of (c) the elastic modulus E and (d) the hardness H as a function of indentation depth h as determined by NI for the amorphous phase, bulk spherulites and TC layers of model test samples.

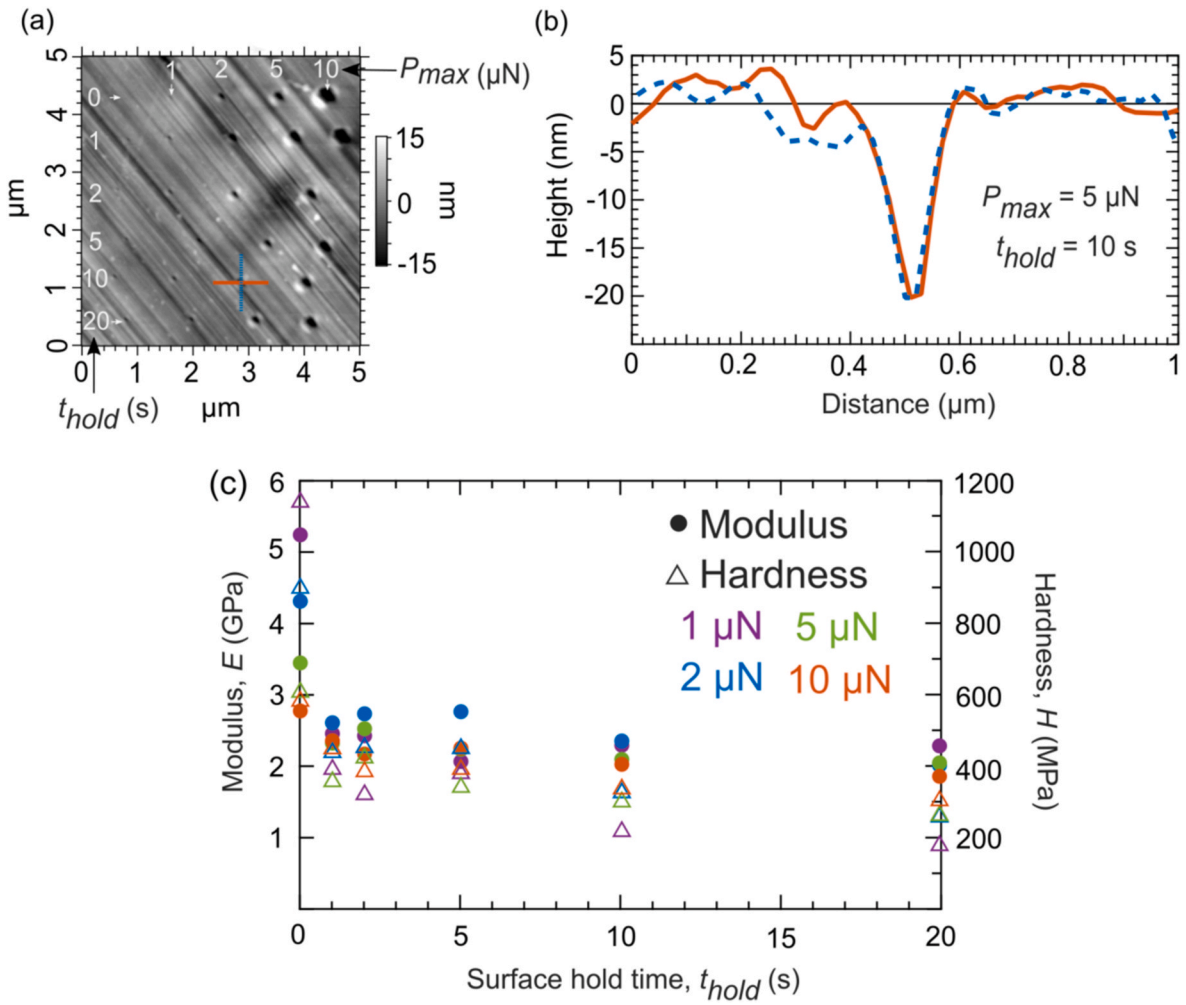

Fig. 4. Results of the atomic force microscopy nanoindentation (AFM-NI) parametric study performed on a polished sample of PEEK. (a) AFM image of indents, (b) topographic profiles across the indent obtained with a maximum load (P_{max}) of 5 μN and a surface hold time (t_{hold}) of 10 s and (c) modulus/hardness evolution with P_{max} and t_{hold}.

amorphous phase/spherulite interface is given in Fig. 5(b) and (d), respectively. Fig. 5(f) focuses on the evolution of the mechanical properties through a TC layer and the amorphous phase/TC layer interface. The RMS (root mean square) roughness measured on each topographic image in Fig. 5 is respectively equal to (a) 31 nm, (c) 2.6 nm and (e) 6.3 nm, highlighting that the roughness of the back-surface is lower than at the upper-surface.

The elastic modulus and hardness measurements on a spherulite on the upper surface (Fig. 5(b)) are more dispersed than the ones on a spherulite on the back surface (Fig. 5(d)). The standard deviation associated to the elastic modulus measured on the upper surface is equal to 0.9 GPa and is reduced to 0.3 GPa on the back surface. Regarding the hardness values, the standard deviations are respectively equal to 193 MPa and 48 MPa.

The elastic modulus and hardness measured in a spherulite and TC layer are larger than the ones measured in the amorphous phase (Fig. 5 (d) and (f)). The mean value of E (resp. H) in the spherulite is ~24 % (resp. 16 %) higher than the one in the surrounding amorphous phase, while the mean value of E (resp. H) in the TC layer is ~30 % (resp. 32 %) higher than in the amorphous phase. The mechanical properties of the TC layer measured very close to the fiber (~1 μm distance) do not seem to be impacted by the proximity of the fiber in view of the similarity of the values of E and H determined further away from the fiber (Fig. 5(f)).

It is worth noticing that the values of E and H obtained by AFM-NI on the upper surface are larger than the ones coming from the back-surface.

4. Discussion

4.1. On the model test specimens

The manufacturing of model samples containing only few fibers enabled the characterization of the microstructure of PEEK in the presence of carbon fibers by polarized light microscopy (PLM) and the identification of the different morphologies (Fig. 2), which is hindered by the high fiber volume fraction in standard composites. Since the observations rely on transmission light mode, a sufficiently small sample thickness is required to distinctly reveal the microstructure. However, the sample thickness should not be too small to avoid substrate effects during indentation experiments (see Section 4.3, factor 2). Data generated on model samples cannot be simply translated as such to the composite level for several reasons addressed in Section 4.4. In addition, other ways to easily remove the glass slide from the model samples should be considered in the future to avoid the use of a release agent which may impact the crystallization of the polymer and the mechanical properties measured at the surface of the specimen.

4.2. On "classical"-NI versus AFM-NI

In order to determine the optimum parameters for AFM-NI analyses, experiments were first performed on a polished pure PEEK sample. Based on the results of these tests, the selected maximum load and

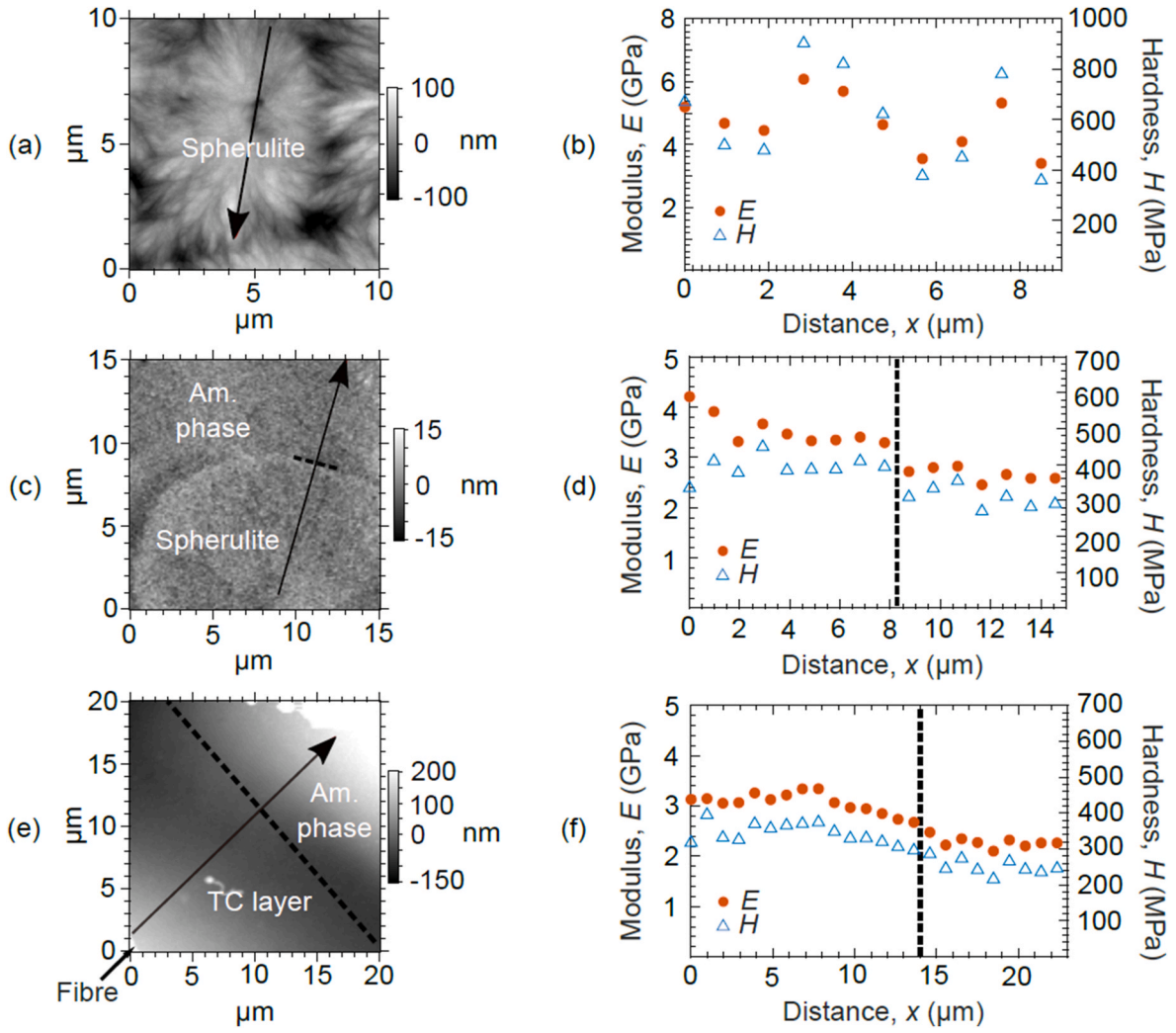

Fig. 5. Topographic images (a, c, e) and modulus/hardness profiles (b, d, f) measured by atomic force microscopy nanoindentation (AFM-NI) along the lines drawn on the images. (a, b) Spherulite (upper surface), (c, d) amorphous phase/spherulite interface (back-surface) and (e, f) amorphous phase/transcrystalline (TC) layer interface (back-surface).

surface hold time were respectively 5 μN and 10 s since larger loads give smaller dispersion on the measured properties. The maximum load was limited to 5 μN because, with the cantilever used in this study, the photodetector response became non-linear above ~6 μN. As shown in Fig. 4(c), the values of the elastic modulus and hardness did not significantly vary for surface hold times larger than 10 s.

The main results obtained by "classical"-NI (or simply "NI") and AFM-NI on the different PEEK morphologies (i.e. amorphous phase, spherulite and TC layers) are given in Fig. 3 et 5 respectively. The added value of AFM-NI is the possibility to probe very locally the mechanical properties of the crystalline structures (Fig. 5), i.e. at the scale of a few lamellae, highlighting a gradient of mechanical properties within crystalline structures in accordance with what was published in Ref. [57], and very close to the fiber (~1 μm distance) without being impacted by the latter (Fig. 5(e and f)).

Fig. 6 summarizes the mean values of (a) E, (b) H and (c) the ratio H/E measured by NI and AFM-NI (on the back-surface) in the different PEEK morphologies. For NI, the data were taken at an indentation depth of 150 nm to avoid both surface and substrate effects (see point 4.3, factors 2). Only the data from the AFM-NI tests on the back-surface were considered here since the values obtained on the upper surface might be overestimated due to a potential contamination of the tip prior to/during testing. The represented data correspond to the mean values obtained in each PEEK morphologies on a series of AFM images taken on the back-surface. The measurements from AFM-NI tests are semi-quantitative due in particular to the challenge of accurately determining the tip shape [24]. The values obtained during the parametric study on the quenched and polished sample of PEEK are also presented for comparison.

The TC layer exhibits the largest E and H, followed by the spherulite and then the amorphous phase. The values obtained by AFM-NI in the TC layer do not follow the trend which is potentially explained by the local higher surface roughness of the TC layer (6.3 nm) compared to the spherulite (2.6 nm) which can affect the measurements. The differences in mechanical properties measured in the three PEEK morphologies may be explained by the variation in the degree of crystallinity. A deeper analysis of the link with the degree of crystallinity is left to further studies. In Fig. 6(c), the values of H/E obtained by both indentation techniques indicate that the level of elastic deformation is almost constant and that the plastic response of PEEK is very much connected to the elastic stiffness, proving the very good consistency between results. The H/E ratio from NI tests are similar to those observed in past studies [10] while the ones obtained from AFM-NI are slightly lower [58]. Finally, the mechanical behavior measured by AFM-NI of the quenched PEEK bulk sample is similar to the one of the amorphous phase in model sample.

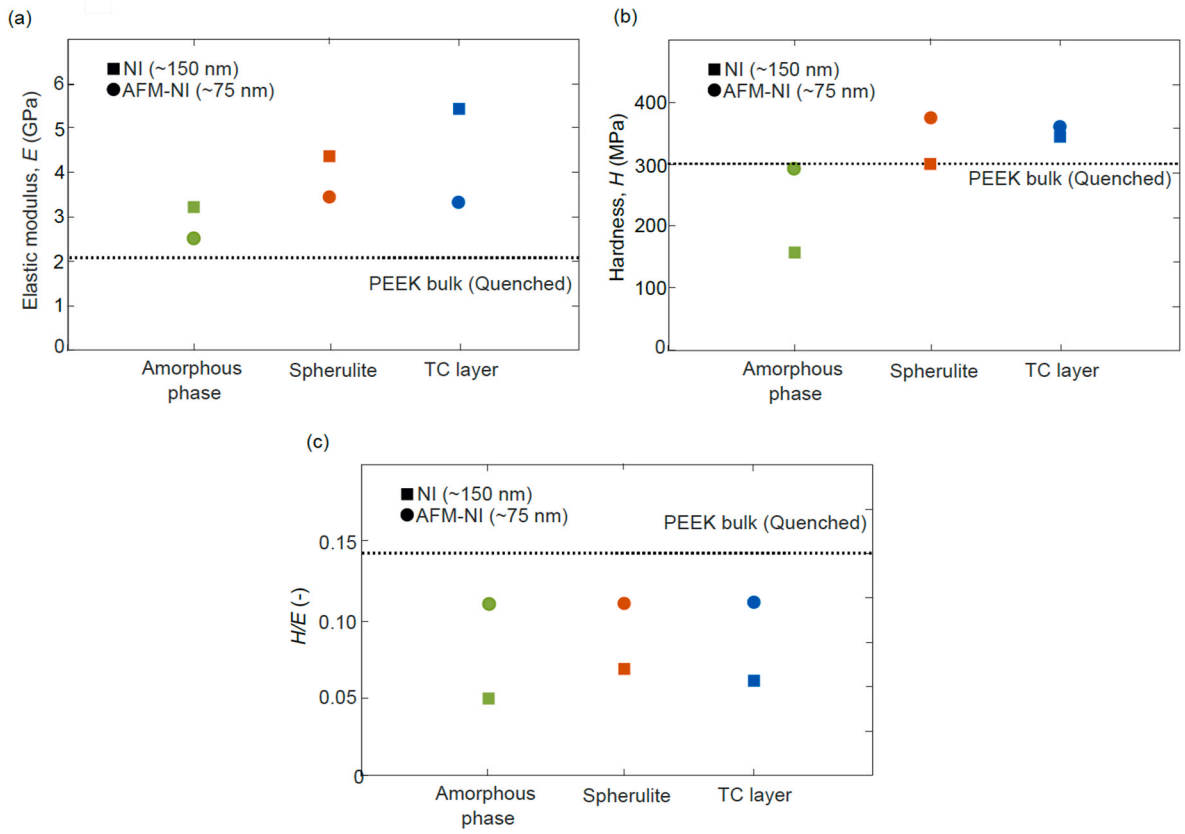

Fig. 6. (a) Elastic modulus (E), (b) hardness (H) and (c) H/E ratio measured by nanoindentation (NI) (corresponding to a depth of 150 nm) and atomic force microscopy nanoindentation (AFM-NI) (on the back surface) in the amorphous phase, bulk spherulites and transcrystalline (TC) layers of model test specimens; the values measured on quenched bulk PEEK specimens during the parametric study of the AFM-NI tests are also added for comparison (dashed line).

4.3. Artefacts and sources of uncertainty

Figs. 3 and 5 highlight that both "classical"-NI and AFM-NI are suitable methods to evaluate the local mechanical properties (i.e. E and H) on the proposed model specimens and to characterize the variations of mechanical behavior in different PEEK morphologies.

However, several factors must be considered and well controlled in order to generate reliable results from indentation experiments; surface roughness, sample thickness and fiber proximity must be carefully considered. Fig. 7 shows a schematic drawing representing the length scale of these parameters as compared to usual dimensions of spherulites and TC layers, while the tip size for both NI and AFM-NI are also represented. Note that the spherulite is not represented as a perfect spherical structure due to the predominant two-dimensional growth within thin polymer films [52].

Factor 1: Surface roughness. The presence of large standard deviations on the elastic modulus and on the hardness could be explained by a possible variation of mechanical properties within crystalline structures. However, the surface roughness also affects the dispersion in the measurements. Minimizing the surface roughness is a key factor to get reliable elastic modulus and hardness measurements, especially when using AFM. ISO standard recommends a roughness smaller than 5 % of the maximum indentation depth, h_{max} [54].

As observed in Fig. 5, the E and H measurements in a spherulite on the upper surface show a higher dispersion than the ones obtained for a spherulite indented from the back-surface, which may be explained by the lower surface roughness of the latter (2.6 vs 31 nm). The roughness of the back-surface is lower thanks to the better contact of the polymer film with the lower glass slide during the manufacturing process. The roughness of the upper surface is also influenced by the semi-free organization of the lamellae within crystalline structures. In both cases, h_{max} varied between 60 and 90 nm. The ISO recommendation [54] was thus met on the back surface but not on the upper one, where the roughness is of the same order of magnitude as the indentation depth.

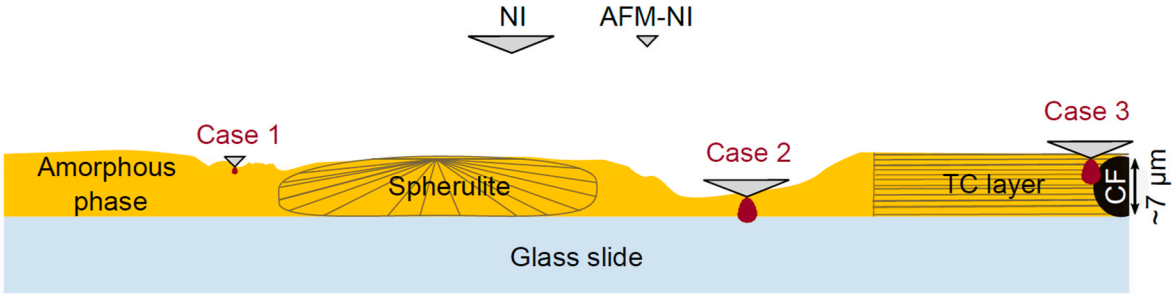

Fig. 7. Schematic summarizing the different factors affecting the values obtained by indentation (i.e. nanoindentation (NI) and atomic force microscopy nanoindentation (AFM-NI)) in thin model samples. The probed volume under an indent is represented as a red bubble.

Obtaining a sufficiently smooth surface roughness on the back surface of model samples without any polishing step is convenient to avoid any alteration of the indented regions. Additionally, the upper surface roughness may also explain the large standard deviations in the measurement of the mechanical properties of crystalline structures with NI (Fig. 3).

Factor 2: Sample thickness. The specimen thickness should be low enough to enable the characterization of the PEEK microstructure with PLM in transmission light mode but not too thin to avoid substrate effects during nanoindentation testing. This typically requires working within a thickness window between a couple of micrometers and 10 μm. This is a range of thickness commensurate with typical fiber diameters. As reported in the literature [59], the sample thickness should be at least 10 times larger than h_{max} to avoid any substrate effect, indicating that a sample should be at least 3 μm thick when indenting up to h_{max} of 300 nm. The one fiber thickness of the sample therefore leads to the appropriate thickness to avoid substrate effects. However, despite an average film thickness in line with the minimum requirements, the lack of true thickness control during the manufacturing process led to variations across the samples, and hence to local values falling below the aforementioned threshold. As a result, several NI results revealed the influence of the substrate before reaching h_{max}, as displayed in Fig. 3(b). Substrate effects could be detected in the NI curves (continuous increase of E (H) with h) corresponding to the amorphous phase and TC layers from an indentation depth of ~150 nm. As a result, the mechanical properties that would be measured beyond this indentation depth cannot be considered as material properties.

Factor 3: Fiber proximity. The proximity of stiff carbon fibers when indenting the TC layers may lead to an overestimation of both E and H [13,60]. In NI tests, the indents were therefore made far enough (i.e. ~10 μm) from the fiber to avoid any influence on the measurements. Indeed, FE simulations of nanoindentation tests have shown that the indentation response is no longer influenced by the presence of the fiber when $x/h > 30$ [12], where x is the distance between the indenter tip and the closest fiber and h is the penetration depth. The selection of an indentation depth of 300 nm therefore hinders the possibility to probe the mechanical properties of the TC layers at distances smaller than 9 μm from the fiber. In AFM-NI, the small tip radius coupled with the lower load enable to measure E and H with lower indentation depths, giving access to the mechanical properties in the TC layers up to very close distances from the fiber (~1 μm or less) without any influence on the results, as shown in Fig. 5(e and f). It is therefore possible with AFM-NI to determine the nanomechanical behavior heterogeneities across the thickness of TC layers.

4.4. Transfer to bulk composite behavior

Extra steps are needed to make use of the data gathered in this study to quantitatively determine the links between the microstructure and mechanical behavior of the interfiber zone of composites, and from there, move to the bulk composite level. Several elements are worth commenting.

- First, the dimensions and organization of the crystalline structures are different in the model samples compared to bulk composites. This is due to the predominant two-dimensional growth of the spherulites within thin polymer films [52] versus the 3D confined growth in composites. The spherulites in the model samples do not exhibit a perfect spherical structure. In addition, due to the smaller interfiber distance in the composite, the development of large crystalline structures as in the model samples is impossible.
- The large volume fraction of carbon fibers in real bulk composite influences the thermal cycles experienced by the matrix. The interfiber distances being larger in model samples, the large thermal conductivity of carbon fibers potentially only influences the thermal cycles experienced by the matrix very close to the fibers while in the composite, the same is true for the whole matrix due to the small interfiber distance. Model samples and composites processed in the same conditions might therefore involve different degrees of crystallinity.
- The differences in the thermal expansion coefficients between the carbon fibers and PEEK can lead to large levels of residual stresses in the composite. These residual stresses may influence the crystallization of the matrix and the mechanical behavior of the interfiber zone.
- It is important to consider heterogeneities at different scales within thicker (~ few mm) composite parts for modeling. First, due to the poor thermal conductivity of PEEK, the thermal cycles experienced by the matrix differs in the core and the edges of the sample, leading to a gradient of degree of crystallinity and microstructure along the sample thickness. In addition, the heterogenous distribution of fibers within the composite leads to the development of different microstructures within the interfiber zones of different dimensions. A combination of TC layers and spherulites might be present in large interfiber zones while smaller interfiber regions might significantly restrict crystallization outside of TC layers. Finally, the formation of TC layers at the fiber/matrix interface is influenced by additional parameters that vary locally (pressure, cooling rate, nature of the fiber/matrix system, …[61–63]) and it cannot therefore be assumed that, in thermal conditions that favor the development of TC layers, the latter is present at each fiber/matrix interface in simulations.

5. Conclusion

The use of polarized light microscopy (PLM) in transmission light mode combined with indentation methods (i.e. NI and AFM-NI) on thin PEEK/CF model samples has proven effective to determine the microstructure and local mechanical behavior of the different morphologies that are encountered in the matrix of PEEK/CF composites.

PLM allows the direct observation of the microstructure of thin PEEK films in the presence of fibers to determine regions of interest for indentation experiments, i.e. “classical”-NI and AFM-NI. Both NI and AFM-NI experiments provide quantitative data regarding the local elastic modulus and hardness of the different PEEK morphologies observed in PLM micrographs. “Classical”-NI showed that, at an indentation depth of 150 nm, the elastic modulus (respectively hardness) of the transcrystalline layers is ~30 % higher (resp. ~15 %) compared to spherulites which are themselves ~35 % (resp. ~ 90 %) stiffer compared to the amorphous phase. AFM-NI also highlighted the larger elastic modulus and hardness in a spherulite and TC layer with a mean elastic modulus (resp. hardness) ~24 % (resp. 16 %) and ~30 % (resp. 32 %) higher than in the surrounding amorphous phase. In order to avoid measurement artefacts, the model specimen must meet several criteria which involve: i) a small surface roughness compared to the maximum indentation depth and ii) a sufficient thickness (ideally ~ 5–10 μm) to avoid substrate effects, but low enough to characterize the microstructure in transmission light mode. Despite a more stringent surface roughness requirement, the added value of AFM-NI compared to “classical”-NI is its capacity of indenting very locally thanks to a small tip radius around a few tens of nanometers and to the low applied load on the order of few μN. In AFM-NI, the volume of material probed under the tip is much smaller than in NI, hence significantly reducing the influence of the close environment, i.e. glass substrate and carbon fibers, on the measurements and enabling the determination of mechanical behavior in TC layers in the vicinity of the fibers, and to perform enough indentations in the zones of interest to ensure the representativity of the results.

The main contribution of this work is to directly correlate the microstructure owing to PLM with advanced nano/micro-mechanical characterization techniques (NI and AFM-NI) on the PEEK/CF system in order to determine the local mechanical behavior of PEEK away from (~few tens of μm) or close to (~1 μm) the fiber without being impacted

by the latter.

The main perspectives of this study are the following:

- The investigation of other routes for easily removing the glass slide from the model samples to avoid the use of a release agent which may impact the crystallization of the polymer and the near surface mechanical properties measured by indentation techniques. If the use of release agent remains the best option, it would be interesting to study its potential influence on the mechanical behavior.
- The study of nano-/micromechanical response of a series of crystalline morphologies, potentially grown at different temperatures, identified from PLM images (i.e. spherulites and TC layers) in order to determine potential differences in elastic modulus and hardness values between and within these crystalline structures.
- The application of the approach to deal with ageing effects that will be very much accelerated owing to the small thickness of the ideal samples proposed in this study.

CRediT authorship contribution statement

Sophie Vanpée: Writing – original draft, Validation, Methodology, Investigation, Conceptualization, Formal analysis, Visualization, Writing – review & editing. **Bernard Nysten:** Validation, Supervision, Investigation, Conceptualization, Formal analysis, Resources, Visualization, Writing – original draft, Writing – review & editing. **Jérémy Chevalier:** Supervision, Resources, Writing – original draft. **Thomas Pardoen:** Supervision, Conceptualization, Resources, Writing – original draft, Writing – review & editing.

Declaration of competing interest

The authors declare that they have no known competing financial interests or personal relationships that could have appeared to influence the work reported in this paper.

Acknowledgments

We gratefully acknowledge the Brussels-Capital Region - Innoviris (Brussels Public Organization for Research and Innovation) for a fellowship for Sophie Vanpée under grant number 2021-PHD-2. All the ressources have been provided by the Institute of Mechanics, Materials and Civil engineering (iMMC), Institute of Condensed Matter and Nanosciences (IMCN) of the Université catholique de Louvain (UCLouvain) and Syensqo (Brussels). Wael Ballout, Audrey Favache et Cécile D'Haese are acknowledged for their technical help with the PLM, NI and AFM experiments respectively.

Data availability

Data will be made available on request but are subject to Syensqo's authorization

References

[1] J. Varna, R. Joffe, L.A. Berglund, Interfacial toughness evaluation from the single-fiber fragmentation test, Compos. Sci. Technol. 56 (1996) 1105–1109, https://doi.org/10.1016/0266-3538(96)00096-6.
[2] S. Kang, D. Lee, N. Choi, Fiber/epoxy interfacial shear strength measured by the microdroplet test, Compos. Sci. Technol. 69 (2009) 245–251, https://doi.org/10.1016/j.compscitech.2008.10.016.
[3] K. Tanaka, K. Minoshima, W. Grela, K. Komai, Characterization of the aramid/epoxy interfacial properties by means of pull-out test and influence of water absorption, Compos. Sci. Technol. 62 (2002) 2169–2177, https://doi.org/10.1016/S0266-3538(02)00147-1.
[4] M. Rodríguez, J.M. Molina-Aldareguía, C. González, J. Llorca, A methodology to measure the interface shear strength by means of the fiber push-in test, Compos. Sci. Technol. 72 (2012) 1924–1932, https://doi.org/10.1016/j.compscitech.2012.08.011.
[5] X.-F. Zhou, H.D. Wagner, S.R. Nutt, Interfacial properties of polymer composites measured by push-out and fragmentation tests, Compos. Part Appl. Sci. Manuf. 32 (2001) 1543–1551, https://doi.org/10.1016/S1359-835X(01)00018-5.
[6] N. Klavzer, S.F. Gayot, M. Coulombier, B. Nysten, T. Pardoen, Nanoscale digital image correlation at elementary fibre/matrix level in polymer–based composites, Compos. Part Appl. Sci. Manuf. 168 (2023) 107455, https://doi.org/10.1016/j.compositesa.2023.107455.
[7] D.G. Yablon, A. Gannepalli, R. Proksch, J. Killgore, D.C. Hurley, J. Grabowski, A. H. Tsou, Quantitative viscoelastic mapping of polyolefin blends with contact resonance atomic force microscopy, Macromolecules 45 (2012) 4363–4370, https://doi.org/10.1021/ma2028038.
[8] M.E. Dokukin, I. Sokolov, Quantitative mapping of the elastic modulus of soft materials with HarmoniX and PeakForce QNM AFM modes, Langmuir 28 (2012) 16060–16071, https://doi.org/10.1021/la302706b.
[9] T. Iqbal, B.J. Briscoe, S. Yasin, P.F. Luckham, Nanoindentation response of poly (ether ether ketone) surfaces-A semicrystalline bimodal behavior, J. Appl. Polym. Sci. (2013), https://doi.org/10.1002/app.39723 n/a-n/a.
[10] G.Z. Voyiadjis, A. Samadi-Dooki, L. Malekmotiei, Nanoindentation of high performance semicrystalline polymers: a case study on PEEK, Polym. Test. 61 (2017) 57–64, https://doi.org/10.1016/j.polymertesting.2017.05.005.
[11] T. Pardoen, N. Klavzer, S. Gayot, F. Van Loock, J. Chevalier, X. Morelle, V. Destoop, F. Lani, P. Camanho, L. Brassart, B. Nysten, C. Bailly, Nanomechanics serving polymer-based composite research, Compt. Rendus Phys. 22 (2021) 331–352, https://doi.org/10.5802/crphys.56.
[12] S.F. Gayot, N. Klavzer, A. Guillet, C. Bailly, P. Gérard, T. Pardoen, B. Nysten, Influence of physical ageing and fibre proximity on the local mechanical response of the Elium® thermoplastic composite matrix, Compos. Part Appl. Sci. Manuf. 181 (2024) 108141, https://doi.org/10.1016/j.compositesa.2024.108141.
[13] S.-L. Gao, E. Mäder, Characterisation of interphase nanoscale property variations in glass fibre reinforced polypropylene and epoxy resin composites, Compos. Part Appl. Sci. Manuf. 33 (2002) 559–576, https://doi.org/10.1016/S1359-835X(01)00134-8.
[14] Y. Wang, T.H. Hahn, AFM characterization of the interfacial properties of carbon fiber reinforced polymer composites subjected to hygrothermal treatments, Compos. Sci. Technol. 67 (2007) 92–101, https://doi.org/10.1016/j.compscitech.2006.03.030.
[15] V. Cech, E. Palesch, J. Lukes, The glass fiber–polymer matrix interface/interphase characterized by nanoscale imaging techniques, Compos. Sci. Technol. 83 (2013) 22–26, https://doi.org/10.1016/j.compscitech.2013.04.014.
[16] M. Zhang, Y. Li, P.V. Kolluru, L.C. Brinson, Determination of mechanical properties of polymer interphase using combined atomic force microscope (AFM) experiments and finite element simulations, Macromolecules 51 (2018) 8229–8240, https://doi.org/10.1021/acs.macromol.8b01427.
[17] M. Griepentrog, G. Krämer, B. Cappella, Comparison of nanoindentation and AFM methods for the determination of mechanical properties of polymers, Polym. Test. 32 (2013) 455–460, https://doi.org/10.1016/j.polymertesting.2013.01.011.
[18] H. Pérez-Martín, P. Mackenzie, A. Baidak, C.M. Ó Brádaigh, D. Ray, Microstructural and micromechanical property characterisation of CF/PEKK composites using nanoindentation, Mater. Des. 234 (2023) 112359, https://doi.org/10.1016/j.matdes.2023.112359.
[19] R. Lesan-Khosh, R. Bagheri, S. Asgari, Nanoindentation of isotactic polypropylene: correlations between hardness, yield stress, and modulus on the local and global scales, J. Appl. Polym. Sci. 121 (2011) 930–938, https://doi.org/10.1002/app.33635.
[20] S. Liparoti, A. Sorrentino, V. Speranza, G. Titomanlio, Multiscale mechanical characterization of iPP injection molded samples, Eur. Polym. J. 90 (2017) 79–91, https://doi.org/10.1016/j.eurpolymj.2017.03.010.
[21] A. Molazemhosseini, H. Tourani, M.R. Naimi-Jamal, A. Khavandi, Nanoindentation and nanoscratching responses of PEEK based hybrid composites reinforced with short carbon fibers and nano-silica, Polym. Test. 32 (2013) 525–534, https://doi.org/10.1016/j.polymertesting.2013.02.001.
[22] Y. Gaillard, F. Amiot, Grid nano-indentation as full-field measurements, Compos. Part Appl. Sci. Manuf. 132 (2020) 105807, https://doi.org/10.1016/j.compositesa.2020.105807.
[23] T. Labour, L. Ferry, C. Gauthier, P. Hajji, G. Vigier, α- and β-crystalline forms of isotactic polypropylene investigated by nanoindentation, J. Appl. Polym. Sci. 74 (1999) 195–200, https://doi.org/10.1002/(SICI)1097-4628(19991003)74:1<195::AID-APP24>3.0.CO;2-8.
[24] J. Grondin, O. Smerdova, S. Castagnet, C. Tromas, Intraspherulitic mechanical heterogeneities and microstructure of i-PP highlighted by nanoindentation and atomic force microscopy, Polymer 285 (2023) 126391, https://doi.org/10.1016/j.polymer.2023.126391.
[25] P. Enrique-Jimenez, J. Vega, J. Martínez-Salazar, F. Ania, A. Flores, Mapping the mechanical properties of poly(3-hydroxybutyrate-co-3-hydroxyvalerate) banded spherulites by nanoindentation, Polymers 8 (2016) 358, https://doi.org/10.3390/polym8100358.
[26] G.Z. Voyiadjis, L. Malekmotiei, A. Samadi-Dooki, Indentation size effect in amorphous polymers based on shear transformation mediated plasticity, Polymer 137 (2018) 72–81, https://doi.org/10.1016/j.polymer.2018.01.006.
[27] P. Christöfl, C. Czibula, M. Berer, G. Oreski, C. Teichert, G. Pinter, Comprehensive investigation of the viscoelastic properties of PMMA by nanoindentation, Polym. Test. 93 (2021) 106978, https://doi.org/10.1016/j.polymertesting.2020.106978.
[28] A. Voss, R.W. Stark, C. Dietz, Surface versus volume properties on the nanoscale: elastomeric polypropylene, Macromolecules 47 (2014) 5236–5245, https://doi.org/10.1021/ma500578e.

[29] X. Wu, S. Shi, Z. Yu, T.P. Russell, D. Wang, AFM nanomechanical mapping and nanothermal analysis reveal enhanced crystallization at the surface of a semicrystalline polymer, Polymer 146 (2018) 188–195, https://doi.org/10.1016/j.polymer.2018.05.043.
[30] Q. Zia, D. Tranchida, R. Androsch, H. Schönherr, Effect of crystal habit and superstructure on modulus of elasticity of isotactic polypropylene by AFM nanoindentation, J. Mater. Sci. 47 (2012) 3040–3045, https://doi.org/10.1007/s10853-011-6135-y.
[31] B. Cappella, G. Dietler, Force-distance curves by atomic force microscopy, Surf. Sci. Rep. 34 (1999) 1–104, https://doi.org/10.1016/S0167-5729(99)00003-5.
[32] H.-J. Butt, B. Cappella, M. Kappl, Force measurements with the atomic force microscope: technique, interpretation and applications, Surf. Sci. Rep. 59 (2005) 1–152, https://doi.org/10.1016/j.surfrep.2005.08.003.
[33] G. Moeller, V. Domnich, AFM nanoindentation of polymers, Microsc. Microanal. 13 (2007), https://doi.org/10.1017/S1431927607073850.
[34] A.-Y. Jee, M. Lee, Comparative analysis on the nanoindentation of polymers using atomic force microscopy, Polym. Test. 29 (2010) 95–99, https://doi.org/10.1016/j.polymertesting.2009.09.009.
[35] D. Tranchida, S. Piccarolo, On the use of the nanoindentation unloading curve to measure the young's modulus of polymers on a nanometer scale, Macromol. Rapid Commun. 26 (2005) 1800–1804, https://doi.org/10.1002/marc.200500538.
[36] C.A. Clifford, M.P. Seah, Quantification issues in the identification of nanoscale regions of homopolymers using modulus measurement via AFM nanoindentation, Appl. Surf. Sci. 252 (2005) 1915–1933, https://doi.org/10.1016/j.apsusc.2005.08.090.
[37] D. Tranchida, S. Piccarolo, M. Soliman, Nanoscale mechanical characterization of polymers by AFM nanoindentations: critical approach to the elastic characterization, Macromolecules 39 (2006) 4547–4556, https://doi.org/10.1021/ma052727j.
[38] D. Tranchida, Z. Kiflie, S. Piccarolo, Viscoelastic recovery behavior following atomic force microscope nanoindentation of semicrystalline poly(ethylene), Macromolecules 40 (2007) 7366–7371, https://doi.org/10.1021/ma070682b.
[39] F. Bédoui, F. Sansoz, N.S. Murthy, Incidence of nanoscale heterogeneity on the nanoindentation of a semicrystalline polymer: experiments and modeling, Acta Mater. 56 (2008) 2296–2306, https://doi.org/10.1016/j.actamat.2008.01.021.
[40] R.E. Mahaffy, S. Park, E. Gerde, J. Käs, C.K. Shih, Quantitative analysis of the viscoelastic properties of thin regions of fibroblasts using atomic force microscopy, Biophys. J. 86 (2004) 1777–1793, https://doi.org/10.1016/S0006-3495(04)74245-9.
[41] J. Zhou, Q. Cai, F. Xu, Nanoscale mechanical properties and indentation recovery of PI@GO composites measured using AFM, Polymers 10 (2018) 1020, https://doi.org/10.3390/polym10091020.
[42] M.A. Monclus, T.J. Young, D. Di Maio, AFM indentation method used for elastic modulus characterization of interfaces and thin layers, J. Mater. Sci. 45 (2010) 3190–3197, https://doi.org/10.1007/s10853-010-4326-6.
[43] J. Gregory, S. Spearing, Nanoindentation of neat and polymers in polymer-matrix composites, Compos. Sci. Technol. 65 (2005) 595–607, https://doi.org/10.1016/j.compscitech.2004.09.001.
[44] M. Hardiman, T.J. Vaughan, C.T. McCarthy, Fibrous composite matrix characterisation using nanoindentation: the effect of fibre constraint and the evolution from bulk to in-situ matrix properties, Compos. Part Appl. Sci. Manuf. 68 (2015) 296–303, https://doi.org/10.1016/j.compositesa.2014.09.022.
[45] M. Hardiman, T.J. Vaughan, C.T. McCarthy, The effects of pile-up, viscoelasticity and hydrostatic stress on polymer matrix nanoindentation, Polym. Test. 52 (2016) 157–166, https://doi.org/10.1016/j.polymertesting.2016.04.003.
[46] M. Pecora, O. Smerdova, M. Gigliotti, In-situ characterization of the local mechanical behaviour of polymer matrix in 3D carbon fiber composites by cyclic indentation test, Compos. Struct. 244 (2020) 112268, https://doi.org/10.1016/j.compstruct.2020.112268.
[47] S.-L. Gao, J.-K. Kim, Crystallinity and interphase properties of carbon fibre/PEEK matrix composites. Proceeding of the 12th International Conference Composite Materials (ICCM-12), 1999, pp. 5–9.
[48] A.J. Waddon, M.J. Hill, A. Keller, D.J. Blundell, On the crystal texture of linear polyaryls (PEEK, PEK and PPS), J. Mater. Sci. 22 (1987) 1773–1784, https://doi.org/10.1007/BF01132406.
[49] W. Wang, Z. Qi, G. Jeronimidis, Studies on interface structure and crystal texture of poly(ether-ether-ketone)-carbon fibre composite, J. Mater. Sci. 26 (1991) 5915–5920, https://doi.org/10.1007/BF01130134.
[50] K. Yu, J. Zhang, G. Liu, J. Yao, H. Liu, C. Chen, Inverse effects of cooling rates on the interfacial shear strength of carbon Fiber/PEEK composites with and without presence of transcrystal layers, Polymer 302 (2024) 127067, https://doi.org/10.1016/j.polymer.2024.127067.
[51] A. Schlothauer, G.A. Pappas, P. Ermanni, Thin-ply thermoplastic composites: from weak to robust transverse performance through microstructural and morphological tuning, Composites, Part B 261 (2023) 110764, https://doi.org/10.1016/j.compositesb.2023.110764.
[52] B. Crist, J.M. Schultz, Polymer spherulites: a critical review, Prog. Polym. Sci. 56 (2016) 1–63, https://doi.org/10.1016/j.progpolymsci.2015.11.006.
[53] W.C. Oliver, G.M. Pharr, An improved technique for determining hardness and elastic modulus using load and displacement sensing indentation experiments, J. Mater. Res. 7 (1992) 1564–1583, https://doi.org/10.1557/JMR.1992.1564.
[54] D.A. Lucca, K. Herrmann, M.J. Klopfstein, Nanoindentation: measuring methods and applications, CIRP Ann 59 (2010) 803–819, https://doi.org/10.1016/j.cirp.2010.05.009.
[55] A. Charvátová Campbell, Z. Geršlová, V. Šindlář, R. Šlesinger, G. Wimmer, New framework for nanoindentation curve fitting and measurement uncertainty estimation, Precis. Eng. 85 (2024) 166–173, https://doi.org/10.1016/j.precisioneng.2023.10.001.
[56] A.M. Díez-Pascual, M.A. Gómez-Fatou, F. Ania, A. Flores, Nanoindentation in polymer nanocomposites, Prog. Mater. Sci. 67 (2015) 1–94, https://doi.org/10.1016/j.pmatsci.2014.06.002.
[57] N. Selles, P. Cloetens, H. Proudhon, T.F. Morgeneyer, O. Klinkova, N. Saintier, L. Laiarinandrasana, Voiding mechanisms in deformed polyamide 6 observed at the nanometric scale, Macromolecules 50 (2017) 4372–4383, https://doi.org/10.1021/acs.macromol.7b00727.
[58] Y. Yang, Sensitivity of nanoindentation strain rate in poly(ester-ester-ketone) using atomic force microscopy, Polym. Test. 53 (2016) 85–88, https://doi.org/10.1016/j.polymertesting.2016.05.013.
[59] T.Y. Tsui, G.M. Pharr, Substrate effects on nanoindentation mechanical property measurement of soft films on hard substrates, J. Mater. Res. 14 (1999) 292–301, https://doi.org/10.1557/JMR.1999.0042.
[60] S.-H. Lee, S. Wang, G.M. Pharr, H. Xu, Evaluation of interphase properties in a cellulose fiber-reinforced polypropylene composite by nanoindentation and finite element analysis, Compos. Part Appl. Sci. Manuf. 38 (2007) 1517–1524, https://doi.org/10.1016/j.compositesa.2007.01.007.
[61] H. Quan, Z.-M. Li, M.-B. Yang, R. Huang, On transcrystallinity in semi-crystalline polymer composites, Compos. Sci. Technol. 65 (2005) 999–1021, https://doi.org/10.1016/j.compscitech.2004.11.015.
[62] C. Wang, C.-R. Liu, Transcrystallization of polypropylene composites: nucleating ability of fibres, Polymer 40 (1999) 289–298, https://doi.org/10.1016/S0032-3861(98)00240-7.
[63] J.P. Abdou, G.A. Braggin, Y. Luo, A.R. Stevenson, D. Chun, S. Zhang, Graphene-induced oriented interfacial microstructures in single fiber polymer composites, ACS Appl. Mater. Interfaces 7 (2015) 13620–13626, https://doi.org/10.1021/acsami.5b03269.